

A species-level model for metabolic scaling of trees

II. Testing in a ring- and diffuse-porous species

Erica I. von Allmen¹, John S. Sperry^{*1}, Duncan D. Smith¹, Van M. Savage², Brian J. Enquist³, Peter B. Reich^{4,5} and Lisa P. Bentley³

¹Department of Biology, University of Utah, Salt Lake City, Utah, 84112 USA; ²Department of Biomathematics, Department of Ecology and Evolutionary Biology, David Geffen School of Medicine, University of California, Los Angeles, California, 90095 USA; ³Department of Ecology and Evolutionary Biology, University of Arizona, Tucson, Arizona, 85721 USA; ⁴Department of Forest Resources, University of Minnesota, St. Paul, Minnesota, 55108 USA; and ⁵Hawkesbury Institute for the Environment, University of Western Sydney, Penrith, New South Wales, 2751 Australia

Summary

1. A 17-parameter ‘species model’ that predicts metabolic scaling from vascular architecture was tested in a diffuse-porous maple (*Acer grandidentatum*) and a ring-porous oak (*Quercus gambelii*). Predictions of midday water transport (Q) and its scaling with above-ground mass (M) were compared with empirical measurements. We also tested the assumption that Q was proportional to the biomass growth rate of the shoot (G).

2. Water transport and biomass growth rate were measured on 18 trees per species that spanned a broad range in trunk diameter (4–26 cm). Where possible, the same trees were used for obtaining the 17 model parameters that concern external branching, internal xylem conduit anatomy, and soil-to-canopy sap pressure drop.

3. The model succeeded in predicting the Q by M^b scaling exponent, b , being within 8% (maple) and 6% (oak) of measured exponents from sap flow data. In terms of absolute Q , the model was better in maple (16% Q overestimate) than oak (128% overestimate). The overestimation of Q was consistent with the model not accounting for cavitation, which is reportedly more prevalent in oak than in maple at the study site.

4. The modelled and measured Q by M^b exponents averaged within 3.6% of the measured G by M^b exponents, supporting the assumption that $G \propto Q^1$. The average b exponent was 0.62 ± 0.016 (mean \pm SE) across species, rejecting $b = 0.75$ for intraspecific scaling.

5. The performance of this species model, both for scaling purposes as well as for predicting rates of water consumption within and between species, argues for its further refinement and wider application in ecology and ecosystem biology.

Key-words: allometry, ecohydrology, hydraulic architecture, metabolic scaling theory, plant water transport, ring-porous and diffuse-porous trees, sap flow, vascular networks, WBE model

Introduction

Botanical ‘metabolic scaling’ theory has potential for linking the anatomy, morphology and physiology of plants with ecosystem fluxes of water and carbon (Enquist *et al.* 2007). The framework established by West Brown and Enquist (WBE; West, Brown & Enquist 1997, 1999) predicts plant water use and growth rate from a basic model of plant branching and internal vascular plumbing. The model has seen several refinements (Enquist, West &

Brown 2000; Price, Enquist & Savage 2007), most recently in the work of Savage *et al.* (2010), which incorporates the inverse relationship between xylem conduit diameter and number per area (Sperry, Meinzer & McCulloh 2008). The first paper of this series presents further development of a ‘species model’ with the goal of predicting actual rates of water use across species and functional types in addition to scaling exponents (Sperry *et al.* 2012). In this second paper, we test the species model in two species with very different vascular architecture.

The starting assumption of plant metabolic scaling theory is that metabolic rate is proportional to the rate of

*Correspondence author. E-mail: j.sperry@utah.edu

xylem water transport, Q (West, Brown & Enquist 1999). Under steady-state conditions, Q will approximate the rate of transpiration. Transpiration and CO_2 uptake occur through the same diffusion path at the stomatal pores. Therefore, as long as the rate of photosynthesis is predominantly limited by CO_2 diffusion (rather than by reaction kinetics), contemporaneous transpiration and CO_2 assimilation should, and does, co-vary (Hubbard, Bond & Ryan 1999; Hubbard *et al.* 2001). Carbon assimilated by leaves is allocated to many sinks, including respiration, growth, storage and reproduction. If allocation to growth is size invariant, then biomass growth rate (G), an easily measured metabolic component, would be directly proportional to vascular supply: $G \propto Q$ (an isometric relationship).

The math of metabolic scaling theory is in the derivation of how Q should scale with above-ground tree mass (M): $Q \propto M^b$, where b is the metabolic scaling exponent. The allometry of growth rate with mass then follows: $G \propto Q \propto M^b$.

The derivation of $Q \propto M^b$ scaling in the species model can be broken down into two components. ‘Mass allometry’ describes how trunk diameter (D_{B0} ; Supporting Information I. Table S1 defines symbols) scales with above-ground tree mass:

$$D_{B0} = k_1 M^c \quad \text{eqn 1}$$

The exponent, c , is derived from established principles of area-preserving branching (i.e. da Vinci’s rule; Horn 2000) and elastic similarity (McMahon 1973), following the logic laid down by the WBE and Savage *et al.* predecessors (West, Brown & Enquist 1999; Savage *et al.* 2010). These principles predict a convergence to $c = 0.375$ as trees increase in size, with the only source of variation being the size range under consideration (Savage *et al.* 2010; Sperry *et al.* 2012). In contrast to c , the multiplier k_1 can vary between species because of variation in branch tissue density and the tree’s safety factor from buckling under its own weight.

‘Water use allometry’ specifies how the steady-state rate of midday xylem transport (Q) scales with trunk diameter

$$Q = k_2 D_{B0}^q \quad \text{eqn 2}$$

The Hagen–Poiseuille equation is used to estimate tree hydraulic conductance (K) from the number and dimensions of the xylem conduits in the tree sapwood. The prediction of K yields Q :

$$Q = K(\Delta P - \rho g H) \quad \text{eqn 3}$$

where ΔP is the soil-to-canopy pressure drop at midday, and $\rho g H$ is the pressure balancing the force of gravity on the water column (ρ = water density; g , acceleration of gravity; H , tree height). Prediction of water transport (Q) from conductance (K) yields the water use allometry of eqn 2.

The modifications for the new species model are intended to improve the prediction of water use allometry,

which appears more variable across species than mass allometry (Sperry *et al.* 2012). Combining the two components of mass and water use allometry (eqns 1 & 2) yields the flow rate by mass scaling: $Q \propto M^b$ and hence growth rate by mass scaling: $G \propto Q \propto M^b$, where the metabolic exponent $b = c \cdot q$.

In this paper, we test the species model by obtaining its 17 parameters from two co-occurring populations of tree species with very different xylem architecture. The ring-porous *Quercus gambelii* conducts water through relatively few large diameter earlywood vessels (~50–200 μm) of one growth ring. The diffuse-porous *Acer grandidentatum* uses more numerous small diameter vessels (~25–50 μm) dispersed through multiple rings. While parameterizing the model, we tested the assumptions of da Vinci’s rule and elastic similarity. Model outputs [exponents c and q , tree hydraulic conductance (K) and rate of water transport (Q)] were compared with measured values from the same population. Shoot growth rate by mass scaling ($G \propto M^b$) was measured to see whether $b = c \cdot q$ as predicted from the key metabolic scaling assumption that $G \propto Q^1$.

Materials and methods

STUDY SITE

Natural stands of *Quercus gambelii* Nutt. (oak, hereafter) and *Acer grandidentatum* Nutt. (maple, hereafter) were studied in Red Butte Canyon Research Natural Area ca. 8 km east of Salt Lake City, Utah (40°47' N 111°48' W). The site receives ca. 500 mm of rain annually (Ehleringer *et al.* 1992), mostly as winter snow and spring rain. Summers are predictably dry and sunny.

Sap flow (Q) measurements were conducted in three mixed stands of the two study species (elevation 1660, 1680 and 1730 m) along the riparian corridor of perennial Red Butte Creek. The riparian habitat was chosen to minimize effects of soil moisture stress that could influence soil-to-canopy pressure drop ($\Delta P - \rho g H$) independently of tree height (H) and cause seasonal shifts in vascular conductance via xylem cavitation. At each site, 12 trees were selected with upper canopies in full sun. Sap flow was measured in a total of 18 individuals per species encompassing a wide range of trunk diameter (oak D_{B0} : 4–23 cm, maple D_{B0} : 5–26 cm). The upper end of the diameter range approached the maximum for the area. Where feasible, the model was parameterized with data from the same 18 trees per species. When additional trees were required, they were located in the same riparian corridor.

MODEL INPUTS

Mass allometry inputs and tests of biomechanical assumptions

Mass allometry (Eqn 1) inputs (1–6 in Table 1) concerned tree branching structure and dimensions. It was beyond our scope to model and measure actual branching architecture, so we assumed the symmetric and self-similar structure of Savage *et al.* (2010) and set the daughter/mother branch ratio at $n = 2$. As detailed in the first paper, this structure was assumed to obey area-preserving branching (da Vinci’s rule) and to converge to elastic similarity with size. Under elastic similarity, the safety factor (H_B/H) from the gravitational buckling height (H_B) is size invariant

(McMahon 1973). These assumptions require a daughter/mother branch diameter ratio of $\beta = 0.707$ and length ratio of $\gamma = 0.793$ (Table 1).

To test whether study species met assumptions of area preservation and convergence to elastic similarity, we dismantled an oak ($D_{B0} = 1.35$ cm) and a maple ($D_{B0} = 2.83$ cm). Area preservation was analysed by comparing mother (proximal) and daughter (distal) stem areas at all branching points. Convergence to elastic similarity was evaluated from a log–log plot of each stem diameter against the distance from that diameter to the most distant twig tip. The model predicts that these data should converge with branch size to loglinearity at a slope of $2/3$ (Sperry *et al.* 2012).

The dimensions of the terminal twigs determine the branch lengths and diameters for all the proximal branch ranks. Twig diameter was set to the average diameter at the base of the current year's extension growth from the two dismantled trees. Terminal twig length was set to the value yielding the observed safety factor from buckling (H_B/H ; Table 1). Safety factors were averaged over 64 maples and 51 oaks, including the 18 trees per species used for sap flux measurements ($4 < D_{B0} < 26$ cm). The D_{B0} was calculated from circumference above the root crown, and maximum canopy height (H) was measured with a clinometer and trigonometry. The H_B was calculated according to

Table 1. Summary of model inputs in order of explanation in text. The first three inputs concern branching architecture and come from previous theory by Savage *et al.* (2010); The remaining inputs are empirical (but see Savage *et al.* for theoretical expectation for some of these parameters). The correction factor C (input 14) is an angiosperm-wide average from the literature. The remaining inputs are species specific. Power function inputs (OLS) and means \pm SE were obtained from data. See Table S1 for definition of symbols (Supporting Information I). Vessel diameter (D_C) was represented by the hydraulic mean diameter (see Model Description).

Model input	Maple	Oak
1. Branch number ratio, n	2	2
2. Branch diameter ratio, β	0.707	0.707
3. Branch length ratio, γ	0.793	0.793
4. Twig diameter (mm)	1.36 \pm 0.025	1.83 \pm 0.089
5. Twig length (mm)	105	98
6. Buckling safety factor H_B/H	2.61 \pm 0.06	3.38 \pm 0.11
7. Pith diameter/twig diameter	0.519 \pm 0.013	0.351 \pm 0.029
8. Bark thickness: T_B (mm), D_B (mm)	$T_B = 0.046 D_B^{1.05}$	$T_B = 0.85 D_B^{0.64}$
9. Sapwood function: A_S (mm ²), D_B (mm)	$A_S = 0.787 D_B^{1.86}$	$A_S = 0.067 D_B^{1.21}$
10. Taper function: D_C (μ m), D_B (mm)	$D_C = 14.76 D_B^{0.15}$	$D_C = 15.15 D_B^{0.50}$
11. D_C max (μ m)	42.71 \pm 0.071	145.8 \pm 1.55
12. D_C twig (μ m), from taper function	15.5	21.1
13. Packing function: F (mm ⁻²), D_C (μ m)	$F = 57,510 D_C^{-1.65}$	$F = 5.954 D_C^{-1.10}$
14. C	0.44	0.44
15. K_L/K_T	0.38 \pm 0.038	0.27 \pm 0.065
16. ΔP (MPa)	1.29 \pm 0.03	1.32 \pm 0.04
17. K/K_S	0.58 \pm 0.031	0.87 \pm 0.068

Niklas (1994). To test whether the H by D_{B0} scaling conformed to elastic similarity, we did a reduced major axis (RMA) regression (chosen for its nonbiased slope estimate, Warton *et al.* 2006; see Statistics) of the logged H and D_{B0} data to test whether the slope = $2/3$ as predicted (McMahon 1973).

Water use allometry inputs

Water use allometry (eqn 2; 7–17 in Table 1) required inputs of xylem structure and function. The model specifies the cross-sectional area of each branch segment that is occupied by pith, xylem, and bark (tissues external to the vascular cambium). Pith area was assumed constant from twig to trunk and was determined from the average pith/twig diameter ratio measured on the trees sectioned for the xylem vessel taper and packing inputs (see below). The same trees were used to measure bark thickness, T_B , across a range of branch diameters, D_B . An OLS regression through log-transformed data yielded a power function for predicting T_B from branch diameter, D_B (OLS is preferable to RMA for predicting y axis values from x axis values; Warton *et al.* 2006; see Statistics).

The cross-sectional area of transporting xylem (the sapwood) was determined from measurements of sapwood area (A_S) and branch diameter (D_B). Sapwood area was estimated from sapwood depth assessed in cores taken from the sap flow trees. In the ring-porous oak, sapwood area was the area of the outermost ring of earlywood vessels where most of the transport occurred as verified by dye perfusions during oak sap flow sensor calibrations (Supporting Information V). In maple, sapwood depth and area were determined from *in situ* dye perfusions (Supporting Information V). An OLS regression of log-transformed A_S and D_B data was used to obtain predictions of A_S from D_B for the model (Table 1).

The 'taper function' input predicts the vessel diameter (D_C) of the outermost growth increment from the branch diameter (D_B) using a power function: $D_C \propto D_B^p$, where p is the taper exponent. It represents the widening of vessel diameter in the outermost growth ring as branch diameter increases from twig to trunk (West, Brown & Enquist 1999; Enquist, West & Brown 2000). This axial 'within-ring' taper is mirrored by radial 'across-ring' widening of vessels from pith to cambium. The taper function was obtained from measurements of D_B and average D_C per growth ring (Supporting Information II) in three oak trees ($D_{B0} = 9.2, 10.5, 11.1$ cm) and two maple trees ($D_{B0} = 11.1, 12.3$ cm). The model calculates hydraulic conductivity by assuming all vessels of a circumferential growth increment have equal D_C . Accordingly, the model used the 'hydraulic mean' D_C calculated for the growth ring sample: $D_C = (\sum D_C^4 / \text{vessel number})^{1/4}$. The hydraulic mean D_C corresponds to the vessel lumen of average Hagen–Poiseuille conductivity for the sample. An OLS regression of log-transformed D_C and D_B for all growth ring samples (pooled across growth rings, branches and trees within a species) was used to obtain species' specific predictions of D_C from D_B for the model (Table 1).

The trunk diameter range for the sampled trees (maximum D_{B0} of 11.1–12.3 cm) was found to capture the full range of D_C based on less extensive measurements in the outer rings of larger trees ($14 < D_{B0} < 26$ cm, three trees per species, three sectors per current growth ring). The average D_C from these larger trees provided estimates of the maximum D_C per species (D_C max; Table 1). Taper functions were prevented from allowing $D_C > D_C$ max, which otherwise could happen as D_C is scaled with D_B up to the maximum in the sap flow trees (maximum $D_{B0} = 23$ cm in oak, 26 cm in maple). The vessel diameter of the terminal twig rank (D_C twig; Table 1) was given by the taper function with $D_B =$ twig diameter.

The vessel packing function predicts the vessel number per area (F) from vessel diameter (D_C) using a power function: $F \propto D_C^d$,

where d is the packing exponent (a negative number). As the vessels get wider, their number per area decreases as required to pack conduits into the available wood space (Sperry, Meinzer & McCulloh 2008; Savage *et al.* 2010). The packing function was obtained from the same growth ring measurements of D_C used for the taper function. The vessel number per growth ring area (F) was measured on the same ring sectors sampled for D_C . An OLS regression of log-transformed F and D_C data for all growth ring sectors provided species specific predictions of F from D_C for the modelled trees (Table 1).

All of the above-mentioned inputs are used to calculate the hydraulic conductance of the branch network using the Hagen–Poiseuille equation for laminar flow through cylindrical tubes. To account for additional resistance of inter-vessel pitting, the Hagen–Poiseuille conductance was multiplied by a correction factor, $C = 0.44$, obtained from the literature (Hacke *et al.* 2006; see also Sperry *et al.* 2012). All sapwood vessels were assumed functional (no cavitation).

The hydraulic conductance of leaves was accounted for by assuming proportionality between the parallel conductances of leaves (K_L) with the calculated conductance of their supporting twigs (K_T , the conductance of the distal-most branch rank). The assumed size-invariant K_L/K_T ratio allowed the conductance of the leaf ‘rank’ to be calculated from K_T , which in turn allowed the entire shoot conductance (K_S , branch network plus leaves) to be calculated. The value of K_L/K_T was measured in both species as described in the Supporting Information III.

Root conductance was incorporated using the ratio of whole-tree conductance (K , root and shoot system in series) to shoot conductance (K/K_S ; shoot conductance, $K_S =$ above-ground conductance of stem network plus leaves). At steady state, K/K_S equals the ratio of the shoot pressure drop (ΔP_S , root crown to leaf) to the total soil-to-canopy pressure drop (ΔP). The $\Delta P_S/\Delta P$ was measured on sap flow trees at midday under clear skies, conditions promoting steady-state flow (Supporting Information IV). The K/K_S was used to calculate K from K_S . Midday ΔP was used to calculate midday steady-state Q from modelled K (eqn 3, $\rho g = 0.009781 \text{ MPa m}^{-1}$).

MODEL OUTPUTS AND BOOTSTRAPPING

The mass allometry exponent, c (eqn 1), was determined from the network volume allometry, $V = H D_{B0}^2 \pi/4$, which assumed $V \propto M^1$ within each species. The mass multiplier, k_V , was not specified. Exponent c was the slope of a linear regression through log-transformed V and D_{B0} values computed across the same D_{B0} range measured for sap flow. The c depended only on the size range of modelled trees (Sperry *et al.* 2012; oak D_{B0} : 4–23 cm, maple D_{B0} : 5–26 cm).

The water use allometry exponent (q , Eqn 2) was obtained by linear regression through log-transformed Q and D_{B0} values computed across the D_{B0} range measured for sap flow. Many of the inputs contained uncertainty (Table 1). We used bootstrapping to propagate this uncertainty into the model output of the Q by D_{B0}^q scaling. Data sets for the taper, packing, sapwood area and K_L/K_T inputs were sampled with replacement to obtain 1000 estimates of input parameters. These inputs were bootstrapped because they were shown to be important in previous analysis (Sperry *et al.* 2012). Inputs were drawn at random to parameterize the model and generate a distribution of Q by D_{B0}^q exponents and multipliers ($n = 1000$ model runs). The 95% confidence intervals for the q and $c \cdot q$ distributions (where c was assumed without error) were computed as the 2.5 and 97.5 percentiles of the distribution. Bootstrapped distributions were approximately normal, so their percentile-based confidence intervals are comparable with 95% intervals estimated for measurements of q .

MODEL VALIDATION

Assessing predictions of whole-tree sap flow (Q) and whole-tree conductance (K)

The rate of water transport (Q) was measured in each sap flux tree ($n = 18$ per species) using heat dissipation sensors (Granier 1985). The calibrated sensors measured sap flux density (Q/A_S) at the base of the trunk, which was multiplied by estimated sapwood area (A_S) to obtain whole-tree Q (Supporting Information V). The model predicts midday, steady-state Q under well-watered conditions where transpiration is limited by stomatal regulation of canopy xylem pressure (i.e. maximum ΔP) rather than by low light, soil moisture or low vapour pressure deficit (VPD). Modelled Q was compared with measurements obtained under the same conditions: midday Q on sunny days with mean VPD within 10% of the seasonal maximum, and from periods where predawn xylem pressures were steady and not trending more negative (indicative of soil drought). Midday Q per tree was the average of the top five values (each a 30-min mean) per day, averaged again over days from June through September 2009 that met the above-mentioned conditions.

Daily ΔP and Q per tree were used to calculate daily whole-tree hydraulic conductance K (using Eqn 3) that was averaged over the sampling dates to yield the average K for each tree. The ΔP was interpolated between measurement days.

Empirical scaling of trunk diameter (D_{B0}) with above-ground (shoot) mass (M^c)

The key assumption for measuring the mass- (c) and growth-scaling exponents (b) was that within each species, V is proportional to tree basal area multiplied by height, H . Accordingly, error in the absolute value of our V , M and G estimates would be size invariant and not influence exponents c or b . Empirical estimates of exponent c were obtained from the same tree height (H) by diameter (D_{B0}) data used for determining the height safety factor input (H_B/H) in the model. Log-transformed values of D_{B0} and V were fit with an RMA regression to give the $D_{B0} \propto V^c$ ($= D_{B0} \propto M^c$) scaling exponent, c .

Assessing predictions for scaling of above-ground growth rate (G) with mass (M^b)

Cores at breast height were taken from each of the sap flow trees to reconstruct the relationship between D_{B0} and year. This was converted to shoot volume growth per year ($\Delta V \text{ year}^{-1}$) from D_{B0} by V^c allometry. Shoot volume growth was multiplied by wood density (Supporting Information VI) to estimate annual above-ground mass (M) growth rate ($G = \Delta M \text{ year}^{-1}$) over the life of each experimental tree. An RMA regression through the log-transformed G vs. M estimates yielded the scaling exponent, b , for each tree. The exponent was averaged across the 18 trees per species to obtain a species mean b exponent.

The empirical G by M exponent b should be equal to the empirical value of $c \cdot q$ if $G \propto Q^1$ as assumed by theory. We used bootstrapping to propagate uncertainty in the empirical c and q estimates to the $c \cdot q$ product for comparison with the G by M^b exponent. The data sets on H , Q and D_{B0} were sampled with replacement to generate 1000 estimates of c and q . Values were drawn from these estimates at random to generate a distribution of the product $c \cdot q$ ($n = 1000$), and the 95% confidence interval computed as the 2.5 and 97.5 percentile of the distribution.

STATISTICS

Power functions were obtained by ordinary least squares (OLS) or RMA linear regressions through log-transformed data as indicated. Following Warton *et al.* (2006), OLS was used when the purpose was to predict a specific 'y' value from a given 'x' value. This is recommended (by Warton *et al.* 2006) regardless of: (i) whether the 'x' variable is fixed by the investigator or is a random variable, (ii) whether or not 'x' is measured with error and (iii) regardless of causation. An RMA regression was used when the purpose was to predict the slope of the relationship (the scaling exponent).

Standard 't' tests ($P = 0.05$) were used to compare empirical means or regression coefficients between species and to compare measurements with parametric values (e.g. values without error). The 't' test could not be used with the bootstrapped distributions (modelled exponent q and $c \cdot q$, and measured $c \cdot q$). In the case of comparing measured $c \cdot q$ with the core-based $G \propto M^b$ exponent (Fig. 5b from cores), we used two methods of comparison: log likelihood and overlap. To compute log likelihood values, we fit a continuous probability density function to each of the two distributions. The log likelihood for each distribution was computed as the sum of the logged probability densities for each observation ($n = 18$ trees per species). Likelihood values within two units of each other are generally considered to indicate similar distributions (Edwards 1992). To compute the overlap between the two probability density distributions, we integrated their overlapping area. The more similar the distributions, the greater their fraction of overlap (0–1, 1 = same distribution, 0 = no overlap).

We did not compare the modelled vs. measured $c \cdot q$ distribution using these methods because model output lacked measurement error and its distribution was expected to be narrower than measured distributions. Thus, even if the mean model prediction was exactly the same as the measured mean, log likelihood and percentage overlap metrics would indicate dissimilar distributions.

Results

MODEL ASSUMPTIONS AND INPUTS

Area-preserving branching (da Vinci's rule) was supported from comparisons of mother and daughter cross-sectional branch areas. For mother branch diameters above 7 mm,

mother/daughter areas did not differ from the expected ratio of one in both species (Fig. 1; maple mother/daughter = 1.01 ± 0.02 ; oak mother/daughter = 0.97 ± 0.09 ; mean \pm SE). However, for smaller branches (< 7 mm), 't' tests indicate that the mother/daughter ratio was greater than one. This probably resulted from twig dieback, which was prevalent in the study site.

Within-tree relationships between branch diameter (D_B) and maximum distal path length showed the predicted convergence on elastic similarity as D_B increased (Fig. 2, solid symbols). Elastic similarity for larger tree sizes (Fig. 2, dotted line) was confirmed for trees of the size measured for sap flow scaling ($D_{B0} = 4\text{--}26$ cm): in both species, height and diameter relationships had scaling exponents (from RMA regressions) that were not significantly different from the expected value of $2/3$ (Fig. 2, open symbols, maple exponent = 0.64 , oak = 0.69 , confidence intervals in Table 2). Safety factors from buckling (H_B/H) averaged 2.61 ± 0.06 in maple and 3.38 ± 0.11 in oak (mean \pm SE).

Most model inputs (Table 1) were straightforward (β , γ , n , twig diameter and length, C , pith/twig diameter, bark thickness, and sapwood areas), but some require more explanation. The taper function ($D_C \propto D_B^d$; Supporting Information VII, Fig. S1; Table 1) was significantly different between maple and oak. The smaller exponent in maple ($p = 0.15$) than oak ($p = 0.50$) reflected the narrower maximum vessel size in large maple trunks ($D_C \text{ max} = 42.71 \pm 0.071 \mu\text{m}$) vs. oak ($D_C \text{ max} = 145.8 \pm 1.55 \mu\text{m}$). Terminal twig vessel diameter was also smaller in maple at $D_C \text{ twig} = 15.5 \mu\text{m}$ than in oak at $D_C \text{ twig} = 21.1 \mu\text{m}$.

Packing functions ($F \propto D_C^d$; Supporting Information VII, Fig. S2, Table 1) were significantly different between species. The maple packing exponent, $d = -1.65$, was less negative than $d = -2$, indicating that larger vessels in major branches occupied a greater percentage of wood space than smaller vessels in twigs. This trend was stronger in oak ($d = -1.10$) where larger branches had growth rings of earlywood vessels with little latewood.

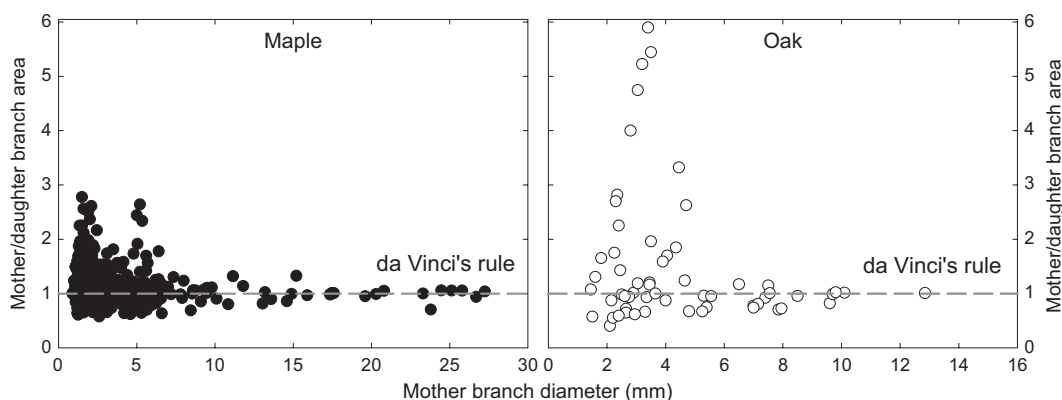


Fig. 1. Comparison of mother stem diameter (mm) and mother/daughter stem area ratio in oak (*Quercus gambelii*, open symbols) and maple (*Acer grandidentatum*, closed symbols). da Vinci's rule (dashed line) assumes a mother/daughter stem area ratio of 1 (area-preserving branching).

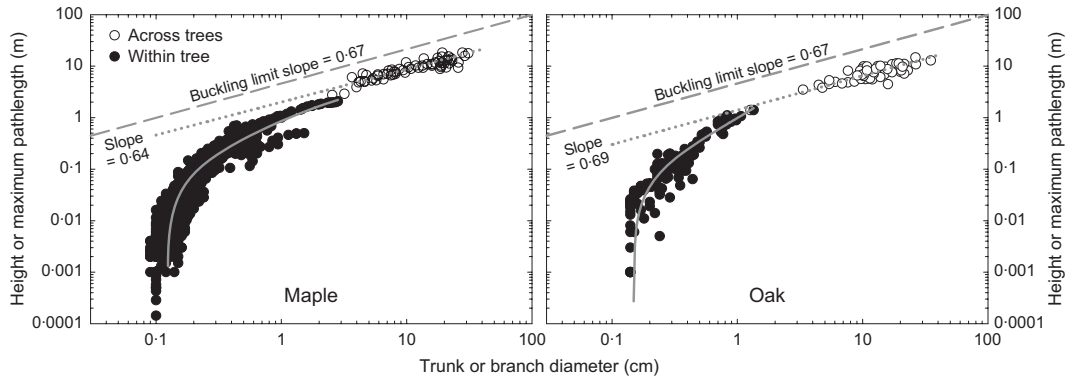


Fig. 2. Log-log plot of trunk (D_{B0}) or branch diameter (D_B) vs. height (H) or maximum path length in oak (*Quercus gambelii*) and maple (*Acer grandidentatum*). Open symbols are D_{B0} and H data from individual trees of the size range measured for sap flow scaling; dotted RMA regression lines are extended to visualize the similarity in slope to the $2/3$ slope of the upper dashed gravitational buckling limit (tree height at elastic buckling, H_B). Solid symbols are D_B vs. path length data within a single smaller tree of each species with a curve fitted to illustrate the trend.

The leaf-to-twigg hydraulic conductance ratio (K_L/K_T) averaged 0.38 ± 0.038 ($n = 5$; mean \pm SE) in maple vs. 0.27 ± 0.065 ($n = 4$) in oak. We excluded an outlier in oak that had an exceptionally high ratio compared with the others (3.9 vs. 0.27). The outlier was caused by an extremely high K_L that was consistent with observed petiole breakage that probably occurred during insertion of the twig into the vacuum canister (Supporting Information III).

The soil-to-canopy pressure drop (ΔP) was independent of tree height as assumed by the model. The ΔP was not different between species (maple = 1.29 ± 0.03 MPa, oak = 1.32 ± 0.04 MPa; mean \pm SE; Table 1). The $\Delta P_S/\Delta P$ was also independent of tree size for both species and was used as an estimate of the size-invariant K/K_S for the model (Table 1). Maple's $\Delta P_S/\Delta P$ averaged 0.58 ± 0.031 (58% of tree hydraulic resistance in shoots). Oak had a much higher ratio of 0.87 ± 0.068 (87% of tree resistance in the shoot).

MODEL VALIDATION

Table 2 summarizes predicted vs. measured scaling exponents. The measured estimates of trunk diameter by mass scaling ($D_{B0} \propto M^c$) exponent c were very close to modelled

predictions in both maple (measured $c = 0.39$ vs. modelled $c = 0.37$) and oak (measured $c = 0.38$ vs. modelled $c = 0.37$; Table 2). This was not surprising given the strong support for area-preserving branching and elastic similarity.

With regard to water use, the model was more precise in predicting the observed Q by D_{B0}^q scaling in maple than in oak (Fig. 3). Predicted Q averaged 1.16 ± 0.075 times measured Q for maple vs. 2.28 ± 0.346 in oak (Fig. 3). The predicted exponent q was 4.4% less than measured for maple vs. 15% greater in oak (Fig. 3). Nevertheless, the measured RMA Q by D_{B0}^q regression line was not different from the model in either species, although for oak, this was the result of its greater measurement variation rather than model accuracy.

The tendency for the model to overestimate Q and q in oak resulted from its overestimation of tree hydraulic conductance (K) in that species (Fig. 4). Although modelled K was directly proportional to measured K in oak (intercept in Fig. 4 not different from zero), the modelled K averaged 2.29 ± 0.321 times the measured K . Modelled K in maple was much closer at 1.36 ± 0.094 times measured K . The $(\Delta P - \rho g H)$ term (Eqn 3) was not different between species, and study trees were short enough (Fig. 2) that Q scaled nearly isometrically with K (Table 2).

Table 2. Modelled and measured scaling exponents. Most modelled exponents were essentially without error except for q where uncertainty was captured by bootstrapping. Bootstrapping was also used to determine uncertainty for the measured $c \cdot q$ product. 95% confidence intervals shown in parentheses.

Scaling relationship	MAPLE exponents		OAK exponents	
	Modelled	Measured	Modelled	Measured
$H \propto D_{B0}$	0.67	0.64 (0.57–0.71)	0.67	0.69 (0.59–0.80)
$Q \propto K$	0.96	0.98 (0.91–1.06)	0.98	0.93 (0.86–1.01)
$Q \propto D_{B0}^q$	1.49 (1.39–1.66)	1.56 (1.24–1.88)	1.81 (1.77–1.86)	1.58 (1.05–2.12)
$D \propto M^c$	0.371	0.39 (0.38–0.40)	0.369	0.38 (0.37–0.40)
$G \propto M^{c \cdot q}$	0.56 (0.52–0.61)	0.61 (0.48–0.73)	0.67 (0.65–0.69)	0.63 (0.41–0.83)
$G \propto M^b$	–	0.61 (0.58–0.64)	–	0.66 (0.61–0.71)
$G \propto Q$	1	1.02 (0.66–1.38)	1	1.13 (0.66–1.60)

The model was successful in predicting the observed 1.85-fold greater water use in maple than oak at the low end of the D_{B0} range ($D_{B0} = 4$ cm). However, the model's overestimate of oak's q exponent resulted in an overly steep increase in oak water use with D_{B0} , resulting in similar predicted water use between species at large D_{B0} ($D_{B0} = 26$ cm; Fig. 3, solid lines). In contrast, measured water use in large maples was 2.7 times that in large oaks (Fig. 3, symbols).

Figure 5 and Table 2 summarize the three independent estimates for growth rate by mass scaling (G by M^b): (i) the model prediction from $b =$ modelled $c \cdot q$ exponents, (ii) the empirical prediction from $b =$ measured $c \cdot q$ exponents and (iii) the direct empirical prediction based on empirical G by M^b scaling from tree core data. All three b estimates were similar within and between species (Fig. 5). Mean estimates ranged from $b = 0.56$ to 0.67 , all below the 0.75 value (Fig. 5, dashed line). The overall interspecific average was 0.62 ± 0.016 (mean \pm SE; individual species' means shown as dotted lines in Fig. 5). The model $c \cdot q$ differed by only 8.2% (maple) and 6.0% (oak) from the empirical $c \cdot q$ estimate, supporting the ability of the model to capture the scaling of mass and water transport with tree size. As expected for a theoretical prediction, the modelled distributions were narrower than the measured distributions in both species (Fig. 5, measured vs. modelled $c \cdot q$).

The empirical $c \cdot q$ estimate deviated by 0% (maple) and 4.5% (oak) from the direct estimate from tree core data ($G \propto M^b$). Because both estimates were empirical and subject to the same sources of measurement error, their distributions were similarly broad (Fig. 5; measured $c \cdot q$ and b from cores), and overlapped considerably by 93% in maple and 74% in oak. Log likelihood values were quite similar in maple, being 23.9 (b) vs. 23.3 ($c \cdot q$). Oak was more divergent at 19.8 (b) vs. 14.8 ($c \cdot q$).

The agreement of measured $c \cdot q$ and the direct estimate of b validates the model assumption that $G \propto Q^1$, particularly in maple. The isometry of G and Q was further supported by direct comparison of estimated shoot biomass growth rate from the same year (2009) that the sap flow data were taken. The G estimates required measuring wood density, which was similar in both species (oak = 0.64 ± 0.014 g cm $^{-3}$, maple = 0.64 ± 0.009 g cm $^{-3}$; mean \pm SE). A log-transformed linear regression (RMA) of G by Q was consistent with isometry in both species (Fig. 6; $G \propto Q^{1.02}$, 95% confidence intervals: 0.66–1.38 in maple, $G \propto Q^{1.13}$ 0.66–1.60 in oak). Maple gained less shoot mass on a yearly basis per average instantaneous midday water consumption (1.64 ± 0.21 h year $^{-1}$) vs. oak (0.40 ± 0.09 h year $^{-1}$). Although these rates are proxies (i.e. assumed to be proportional to actual growth rates within a species) and expressed over widely different time frames (annual vs. instantaneous), they suggest maple is less efficient at exchanging water for shoot growth than oak.

Discussion

Given its many assumptions and relatively few inputs (Table 1), the species-level scaling model was remarkably successful at predicting the hydraulic and metabolic scaling exponents despite the very different anatomies of ring-porous and diffuse-porous species (Table 2, Fig. 3). The model also did a reasonable job of predicting the absolute values of whole-tree water use and hydraulic conductance in maple (*Acer grandidentatum*) while tending to overestimate for oak (*Quercus gambelii*; Figs 3 and 4). Nevertheless, the additional inputs that distinguish the species model from its WBE (West, Brown & Enquist 1997) and Savage *et al.* (2010) predecessors bring realistic species-

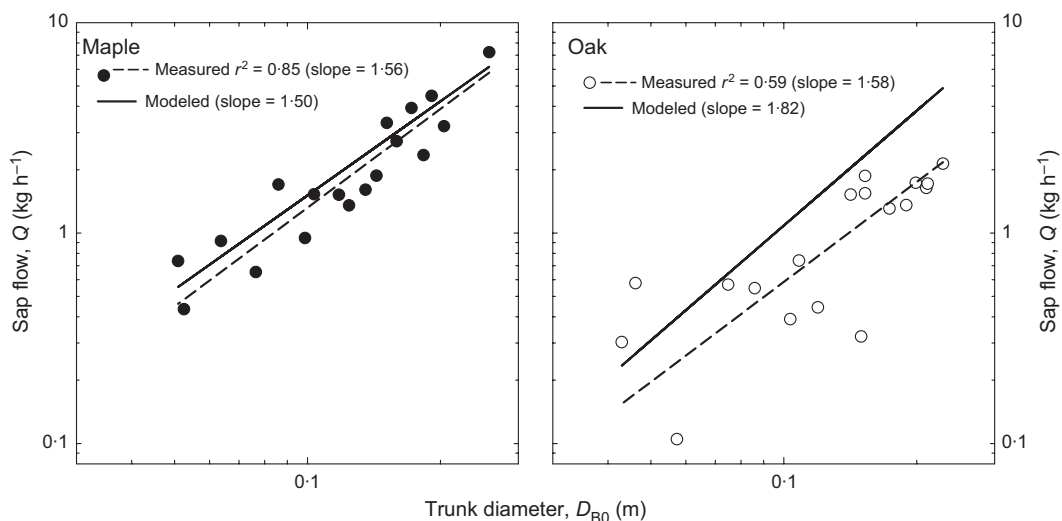


Fig. 3. Log-log scaling of midday sap flow rate (Q) with trunk diameter (D_{B0}) in maple (*Acer grandidentatum*, left) and oak (*Quercus gambelii*, right). Model results are solid lines, measurements are circles and dashed lines are RMA regressions. Measured Q per tree was averaged over selected days during the growing season when conditions maximized transpiration and minimized soil moisture stress.

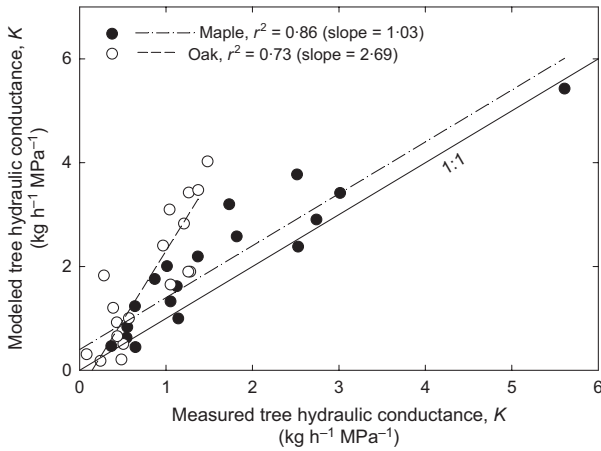


Fig. 4. Log-log comparison of measured vs. modelled whole-tree conductance (K) for maple (*Acer grandidentatum*, solid symbols and dash-dotted RMA regression) and oak (*Quercus gambelii*, open symbols and dashed RMA regression). Measured K per tree was averaged over the same days selected for the average Q (Fig. 3). The 1:1 line is shown.

level predictions of the scaling of actual water use within reach. Our results are the most rigorous test to date of the basic WBE assumption that growth rate scales isometrically with vascular supply capacity ($G \propto Q^1$). Oak and maple showed similar scaling of growth rate with mass, with the various estimates of the $G \propto M^b$ exponent averaging $b = 0.62 \pm 0.016$ across species (mean \pm SE; Fig. 5; Table 2). Both modelled and measured b estimates fell below the canonical $b = 3/4$ -power scaling.

It is convenient to discuss the model's performance progressing from mass allometry (D_{B0} by M^c , Eqn 1) to water use allometry (Q by D_{B0}^q , Eqn 2) and finally to the growth rate by mass scaling prediction ($G \propto Q \propto M^{cq}$). As expected, the prediction of exponent c (D_{B0} by M^c) was well supported, being within 3–5% of measured estimates

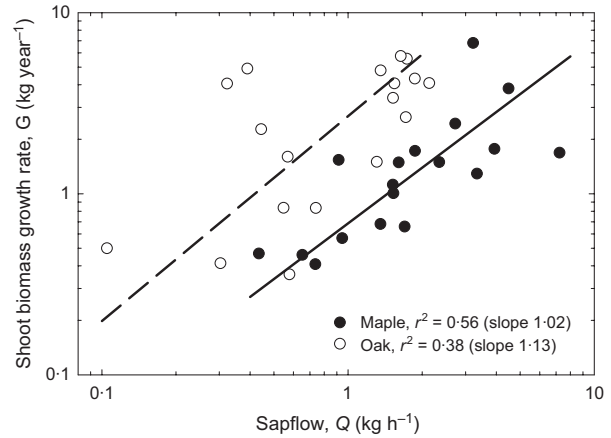


Fig. 6. Log-log plot of estimated shoot biomass growth in 2009 (G) and sap flow (Q) in maple (*Acer grandidentatum*, solid symbols and solid RMA regression) and oak (*Quercus gambelii*, open symbols and dashed RMA regression). These results support the assumption of scaling theory that growth rate and sap flow rate are directly proportional. Maple had less variability in its G by Q scaling ($r^2 = 0.56$) than oak ($r^2 = 0.38$).

(Table 2). This was consistent with the validation of da Vinci's rule (Fig. 1) and the convergence to elastic similarity (Fig. 2). These established concepts are generally supported across a range of species (McMahon 1973; King 1986; Niklas 1994; Horn 2000). We did not evaluate the ability of the model to predict actual values of V and M . Deviations from the assumed self-similar and symmetric branching architecture would lead to errors in V and M predictions (L.P. Bentley, J.C. Stegen, V.M. Savage, B.J. Enquist, D.D. Smith, E.I. von Allmen, J.S. Sperry & P.B. Reich, unpublished). However, as long as any deviation was size invariant, exponent c would be unchanged.

The predicted $Q = k_2 D_{B0}^q$ scaling was chiefly governed by the model calculation of tree hydraulic conductance because of the similarity in the $(\Delta P - \rho g H)$ term between

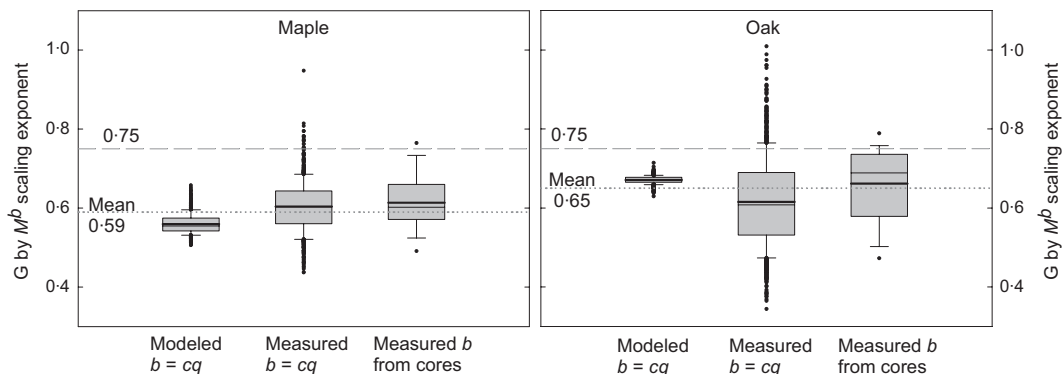


Fig. 5. Box and whisker plots comparing three estimates of the growth rate (G) by shoot mass (M^b) scaling exponent for maple (*Acer grandidentatum*, left) and oak (*Quercus gambelii*, right). The model estimates (left in panel) are $b = cq$ from modelled values of c and q exponents. The measured $b = cq$ (centre in panel) are from measured estimates of c and q exponents. Both c - q distributions were bootstrapped ($n = 1000$) to obtain the distribution. Direct measurement of b (right in panel) was estimated from tree cores. The heavy solid line within each box is the mean, the lighter line is the median, the box is the middle two quartiles (25–75 percentiles), and the bars are the 10 and 90th percentile range. Outliers are shown by symbols. The exponent of 0.75 is shown as a dashed line. Mean of the tree exponents per species is indicated by the dotted line.

the two species ($Q = K [\Delta P - \rho g H]$; eqn 3). The better prediction of water use in maple vs. the overestimate for oak was not unexpected, given the results of research on xylem cavitation in these two species at the same field site (Taneda & Sperry 2008; Christman *et al.* 2012). The model does not account for cavitation because it assumes all sapwood vessels are conducting. In maple, this is a minor issue because midday cavitation in *Acer grandidentatum* at this site and season is minimal, accounting for about 10% reduction in branch hydraulic conductance (Taneda & Sperry 2008). This is consistent with the model overpredicting maple water use by an average of 16%.

In oak, however, midday cavitation in current year's earlywood vessels can be substantial even under non-stressed conditions, accounting for over 1/2 reduction in branch hydraulic conductance at the same field site and season (Taneda & Sperry 2008; Christman *et al.* 2012). Hence, the model should overpredict water use in oak by over 2-fold, consistent with the actual 2.28-fold average overestimate. A constant percentage loss of tree hydraulic conductance to cavitation across all oak sizes would explain the proportionality between measured and modelled K (Fig. 4). If most of the cavitated vessels were in the trunk and major branches (where the vessels are largest and presumably most vulnerable), it would lower their conductance closer to that of the distal twig end of the network. Such reduction in the 'bottleneck effect' has been shown to decrease q (Sperry *et al.* 2012) and may explain why measured $q = 1.58$ was less than the modelled $q = 1.81$. Twig dieback (Fig. 1) would tend to have the opposite effect, and perhaps, this is why in maple (where cavitation is minimal), the measured q (1.56) was greater than modelled ($q = 1.49$). The generally greater variability in the oak measurements is also consistent with highly variable stem hydraulic conductances probably caused by cavitation (Christman *et al.* 2012). Apparently, the efficiency of large vessels in *Quercus gambelii* comes at the cost of their potentially greater vulnerability to cavitation, as predicted for a safety vs. efficiency trade-off in xylem architecture (Hacke *et al.* 2006; Christman *et al.* 2012).

Although the model estimates of Q were generally not as accurate as the Q by D_{Bo}^q scaling exponent, the fact that Q predictions were as close as they were (especially if effects of cavitation are considered) was surprising given the simplicity of the model. Contributing to model accuracy was the incorporation of three empirical 'correction factors' that account for 1) conduit end-walls (C ; Table 2), 2) leaf conductance (K_L/K_T ; Table 2) and 3) root conductance (K/K_S ; Table 2). In principle, the model can be applied to any anatomical type, including conifers (Sperry *et al.* 2012). At the stand and ecosystem scale, the model could be useful for setting upper limits to predictions of stand or watershed water use (Novick *et al.* 2009). Nevertheless, important sources of uncertainty remain. In addition to the cavitation issue, the model does not account for the presence of extra-vascular resistances in root and leaf. The model is also not designed to predict effects of soil

drought, which would alter ΔP and increase cavitation-related error.

Perhaps, the most obvious limitation of the current model is the highly simplified representation of tree branching structure. Although symmetrically self-similar branching may be appropriate for some species, many trees generally show asymmetric branching (Zimmermann & Brown 1977). Indeed, some of the same oak and maple trees we dismantled for testing elastic similarity and area preservation were analysed for deviation from self-similar WBE architecture in a separate study (L.P. Bentley, J.C. Stegen, V.M. Savage, B.J. Enquist, D.D. Smith, E.I. von Allmen, J.S. Sperry & P.B. Reich, unpublished). Preliminary modelling suggests that altering branching structure has more impact on the prediction of absolute values (e.g. the scaling multiplier) than on scaling exponents (D. Smith and J. Sperry, unpubl.; see also Turcotte, Pelletier & Newman 1998). A logical next step in model improvement is the incorporation of variable branching architecture that still conforms to the constraints of area preservation and elastic similarity.

The model was quite successful in predicting the scaling of water use with tree mass: $Q \propto M^{c \cdot q}$, where $c \cdot q$ estimates were within 8.2% of measured $c \cdot q$ values in both species. For these trees, all estimates of the mass scaling exponent were below 3/4 (Fig. 5), and the average of 0.62 was very similar to a global average of $c \cdot q = 0.63$ predicted by the same model applied across temperate and tropical angiosperms and temperate conifers (Sperry *et al.* 2012). These results are also consistent with previous intraspecific estimates in the 0.50–0.66 range (Mencuccini 2003; Sperry, Meinzer & McCulloh 2008). Earlier data suggesting $c \cdot q \approx 0.75$ were chiefly based on interspecific data (Enquist, Brown & West 1998; Niklas & Enquist 2001). As we show in the first paper of this series, interspecific mass scaling can have a larger exponent than intraspecific scaling if larger species are biased towards having greater water transport Q and scaling exponent q than smaller species. However, this hypothesis has not been tested.

The starting assumption of metabolic scaling theory is that growth rate will scale isometrically with water transport: $G \propto Q^1$. This is the rationale for predicting Q from vascular structure in the first place, so that metabolic scaling can be predicted from the chain of proportionalities: $G \propto Q \propto M^{c \cdot q}$ (Enquist, West & Brown 2000). Two linked lines of evidence supported the $G \propto Q^1$ assumption. The first is that measured $Q \propto M^{c \cdot q}$ scaling agreed extremely well with direct measurements of $G \propto M^b$ scaling: the $c \cdot q$ exponent was within 0% (maple) and 4.5% (oak) of the b estimated from tree core data (Fig. 5). This could only happen if G was nearly isometric with Q . The second line of evidence is that plotting estimates of annual G against Q yielded scaling exponents of 1.02 (maple) and 1.13 (oak): within 2–13% of isometry (Fig. 6).

The approximate isometry of growth rate and water use in the two study species is a surprisingly simple outcome of a very complex chain of events. Transpiration presum-

ably must be isometric with net CO₂ uptake, which requires CO₂ uptake to be diffusion limited rather than reaction limited; in turn, this implies coordination between resource allocation (primarily nitrogen) to photosynthetic biochemistry and the supply of water to the leaf. Net assimilation is distributed to net biomass growth in the shoot (G) and the root, as well as to respiration, reproduction, storage, volatile compounds, root exudation and loss of parts. For G to scale isometrically with Q , all of these other allocations must be isometric with G or else show compensatory allometries. The latter may be the case, because whole plant respiration has been shown to increase almost isometrically with mass, at least interspecifically (Reich *et al.* 2006).

Extending the model to include carbon allocation could account for these complexities (Enquist *et al.* 2007) and would allow the model to predict absolute growth rate (G) values for a species as well as sap flow rate (Q), making it even more of a useful tool. Such a model could explain why maple uses more water than oak even though the two species appear to have similar shoot mass growth rates (G ; Fig. 6). Possibly, maple allocates less assimilated carbon to its shoot or has a lower rate of carbon assimilation relative to transpiration (lower instantaneous water use efficiency) than oak.

In conclusion, our results strongly support the starting assumption of metabolic scaling theory that growth rate is proportional to vascular supply. The inclusion of more specific details and thus greater realism of the species model relative to its WBE and Savage *et al.* predecessors (Enquist, West & Brown 2000; Savage *et al.* 2010) allows more accurate predictions of species' and size-specific scaling exponents and has the important advantage of predicting scaling multipliers. Intraspecific $3/4$ -power scaling of water use and growth rate with shoot mass was rejected in the two study species. The model provided reasonably accurate predictions of interspecific differences in plant hydraulic conductance and water use from relatively few parameters. However, accounting for xylem cavitation would further improve its accuracy. The success of the model argues for extending it to account for more flexible branching architectures and more detailed carbon allocation. The potential utility of applying metabolic scaling theory to a more detailed and species-specific model is diverse, expanding beyond allometric studies to analysis of ecophysiology and ecological interactions, ecohydrology and ecosystem processes.

Acknowledgements

We thank Henry Grover, Andy Crowl and David Love for their field assistance; Susan Bush and Kevin Hultine for their technical support of sap flow measurements and calibrations; and Mairgareth Christman for the laboratory assistance. Fred Adler (University of Utah) helped tremendously with data analysis and interpretation. The authors were supported from NSF-ATB-0742800; JSS, EIV and DDS received additional funding from NSF-IBN-0743148. L.P.B. received additional funding from an NSF Postdoctoral Fellowship in Bioinformatics DBI-0905868.

References

- Christman, M.A., Sperry, J.S. & Smith, D.D. (2012) Rare pits, large vessels, and extreme vulnerability to cavitation in a ring-porous tree species. *New Phytologist*, **193**, 713–720.
- Edwards, A.W.F. (1992) *Likelihood*. John Hopkins University Press, London.
- Ehleringer, J.R., Arnow, L.A., Arnow, T., McNulty, I.B. & Negus, N.C. (1992) Red Butte Canyon Research Natural Area: history, flora, geology, climate, and ecology. *Great Basin Naturalist*, **52**, 95–121.
- Enquist, B.J., Brown, J.H. & West, G.B. (1998) Allometric scaling of plant energetics and population density. *Nature*, **395**, 163–166.
- Enquist, B.J., West, G.B. & Brown, J.H. (2000) Quarter-power allometric scaling in vascular plants: functional basis and ecological consequences. *Scaling in Biology* (eds J. H. Brown & G. B. West), pp. 167–198. Oxford University Press, Oxford.
- Enquist, B.J., Kerkhoff, A.J., Stark, S.C., Swenson, N.G., McCarthy, M.C. & Price, C.A. (2007) A general integrative model for scaling plant growth, carbon flux, and functional trait spectra. *Nature*, **449**, 218–222.
- Granier, A. (1985) Une nouvelle methode pour la mesure du flux de seve brute le tronc des arbres. *Annales des Sciences Forestieres*, **42**, 193–200.
- Hacke, U.G., Sperry, J.S., Wheeler, J.K. & Castro, L. (2006) Scaling of angiosperm xylem structure with safety and efficiency. *Tree Physiology*, **26**, 689–701.
- Horn, H.S. (2000) Twigs, trees and the dynamics of carbon in the landscape. *Scaling in Biology* (eds J. H. Brown & G. B. West), pp. 199–220. Oxford University Press, Oxford.
- Hubbard, R.M., Bond, B.J. & Ryan, M.G. (1999) Evidence that hydraulic conductance limits photosynthesis in old *Pinus ponderosa* trees. *Tree Physiology*, **19**, 165–172.
- Hubbard, R.M., Stiller, V., Ryan, M.G. & Sperry, J.S. (2001) Stomatal conductance and photosynthesis vary linearly with plant hydraulic conductance in ponderosa pine. *Plant Cell and Environment*, **24**, 113–121.
- King, D.A. (1986) Tree form, height growth, and susceptibility to wind damage in *Acer saccharum*. *Ecology*, **67**, 980–990.
- McMahon, T.A. (1973) Size and shape in biology. *Science*, **179**, 1201–1204.
- Menuccini, M. (2003) The ecological significance of long-distance water transport: short-term regulation, long-term acclimation and the hydraulic costs of stature across plant life forms. *Plant Cell and Environment*, **26**, 163–182.
- Niklas, K.J. (1994) The allometry of safety-factors for plant height. *American Journal of Botany*, **81**, 345–351.
- Niklas, K.J. & Enquist, B.J. (2001) Invariant scaling relationships for interspecific plant biomass production rates and body size. *Proceedings of the National Academy of Sciences of the United States of America*, **98**, 2922–2927.
- Novick, K.R., Oren, R., Stoy, P., Juang, J.Y., Siqueira, M. & Katul, G. (2009) The relationship between reference canopy conductance and simplified hydraulic architecture. *Advances in Water Resources*, **32**, 809–819.
- Price, C., Enquist, B.J. & Savage, V.M. (2007) A general model for allometric covariation in botanical form and function. *Proceedings of the National Academy of Sciences of the United States of America*, **104**, 13204–13209.
- Reich, P.B., Tjoelker, M.G., Machado, J.L. & Oleksyn, J. (2006) Universal scaling of respiratory metabolism, size and nitrogen in plants. *Nature*, **439**, 457–461.
- Savage, V.M., Bentley, L.P., Enquist, B.J., Sperry, J.S., Smith, D.D., Reich, P.B. & von Allmen, E.I. (2010) Hydraulic trade-offs and space filling enable better predictions of vascular structure and function in plants. *Proceedings of the National Academy of Sciences of the United States of America*, **107**, 22722–22727.
- Sperry, J.S., Meinzer, F.C. & McCulloh, K.A. (2008) Safety and efficiency conflicts in hydraulic architecture: scaling from tissues to trees. *Plant Cell and Environment*, **31**, 632–645.
- Sperry, J.S., Smith, D.D., Savage, V.M., Enquist, B.J., McCulloh, K.A., Reich, P.B., Bentley, L.P. & Von Allmen, E.I. (2012) A species-level model for metabolic scaling of trees I. Exploring boundaries to scaling space within and across species. *Functional Ecology*, doi: 10.1111/j.1365-2435.2012.02022.x.
- Taneda, H. & Sperry, J.S. (2008) A case-study of water transport in co-occurring ring- vs. diffuse-porous trees: contrasts in water-status, conducting capacity, cavitation and vessel refilling. *Tree Physiology*, **28**, 1641–1652.

- Turcotte, D.L., Pelletier, J.D. & Newman, W.I. (1998) Networks with side branching in biology. *Journal of Theoretical Biology*, **193**, 577–592.
- Warton, D.I., Wright, I.J., Falster, D.S. & Westoby, M. (2006) Bivariate line-fitting methods for allometry. *Biological Reviews*, **81**, 259–291.
- West, G.B., Brown, J.H. & Enquist, B.J. (1997) A general model for the origin of allometric scaling laws in biology. *Science*, **276**, 122–126.
- West, G.B., Brown, J.H. & Enquist, B.J. (1999) A general model for the structure and allometry of plant vascular systems. *Nature*, **400**, 664–667.
- Zimmermann, M.H. & Brown, C.L. (1977) *Trees: Structure and Function*. Springer Verlag, New York.

Received 4 October 2011; accepted 17 May 2012

Handling Editor: Niels Anten

Supporting Information

Additional Supporting Information may be found in the online version of this article:

Appendix S1. I. Table S1; II. Taper function; III. Leaf / twig hydraulic conductance ratio; IV. Tree conductance / shoot conductance ratio; V. Sap flow measurements; VI. Wood density measurements; VII. Taper and packing function figures.

As a service to our authors and readers, this journal provides supporting information supplied by the authors. Such materials may be re-organized for online delivery, but are not copy-edited or typeset. Technical support issues arising from supporting information (other than missing files) should be addressed to the authors.